

Numerical Analysis of Steady and Unsteady Sheet Cavitation on a Marine Propeller Using a Simple Surface Panel Method “SQCM”

Takashi Kanemaru¹, Jun Ando²

¹Graduate School of Engineering, Kyushu University, Fukuoka, Japan

²Faculty of Engineering, Kyushu University, Fukuoka, Japan

ABSTRACT

This paper presents a calculation method for the steady and unsteady cavitating propeller problem. The method is based on a simple surface panel method “SQCM” which satisfies the Kutta condition easily. SQCM consists of Hess and Smith type source panels on the propeller or cavity surface and discrete vortices on the camber surface according to Lan’s QCM (Quasi-Continuous vortex lattice Method). The boundary conditions to determine these singularities are the constant pressure condition on the cavity surface and the zero normal velocity condition on the propeller and cavity surfaces.

In this paper, we describe how to apply SQCM to the calculation of nonlinear cavitation on propellers and show some calculated results about cavitation patterns, cavity shapes and cavity volumes in steady and unsteady flow. Good agreements are obtained between the calculated results and published experimental data.

Keywords

SQCM(Source and QCM), Propeller Sheet Cavitation, Free Streamline Theory

1 INTRODUCTION

Cavity on the propeller blade produces the pressure fluctuation on the stern hull surface and also reduces the propeller performance. The recent large container ships give us difficulties in design of propellers because they will operate in heavily loaded condition. Therefore it is important to predict the cavity pattern, volume, and propeller performance accurately.

Panel methods, which can represent the blade shape exactly, are widely used for the prediction of propeller performance. Moreover Kinnas & Fine(1992) and Kim & Lee(1996) presented the cavitation prediction method using panel method.

In Kyushu University we developed a simple surface panel method “SQCM” and applied SQCM to the 2-D and 3-D sheet cavitating hydrofoil problems. SQCM is also expected as an efficient numerical method for cavitating propeller problem. In this paper we extend SQCM to the steady and unsteady cavitating propeller

problem and present the consistent calculation method to treat both the partial cavitation and supercavitation. One of the features in our calculation is that the cross flow velocity near the tip of a propeller blade is taken into consideration at the constant pressure condition on the cavity surface in order to get the reasonable results. We show some calculated results for several kinds of propellers and compare them with the published experimental data. In this paper, we treat the sheet cavitation only.

2 OUTLINE OF SQCM

SQCM (Source and QCM) uses source distributions (Hess & Smith 1964) on the propeller blade surface and discrete vortex distributions arranged on the mean camber surface according to QCM (Quasi-Continuous vortex lattice Method) (Lan 1974). These singularities should satisfy the boundary condition that the normal velocity is zero on the propeller blade and the mean camber surfaces.

Consider a K -bladed propeller rotating with a constant angular velocity Ω ($= 2\pi n$, n : number of propeller revolutions) in inviscid, irrotational and incompressible fluid. The space coordinate system $O-XYZ$ and the propeller coordinate system $o-xyz$ are introduced as **Figure 1**. The cylindrical coordinate system $o-xr\theta$ is also introduced for convenience. Then the following relation transforms the cylindrical coordinate system $o-xr\theta$ into the propeller coordinate system $o-xyz$.

$$x = x, \quad y = -r \sin \theta, \quad z = r \cos \theta \quad (1)$$

Where $r = \sqrt{y^2 + z^2}$, $\theta = \tan^{-1}(-y/z)$

The propeller blade S_B is divided into M panels in the spanwise direction. The face and back surfaces of the blade section are divided into N panels in the chordwise direction, respectively. Therefore the total number of source panels becomes $(M \times 2N) \times K$ and constant source m is distributed in each panel. The velocity vector \vec{V}_m due to the source distributions on the blade surfaces is expressed by using velocity potential Φ_m as

$$\vec{V}_m = \nabla \Phi_m \quad (2)$$

Where $\Phi_m = -\frac{1}{4\pi} \iint_{S_B} \frac{m(x', y', z', t')}{\sqrt{(x-x')^2 + (y-y')^2 + (z-z')^2}} dS$

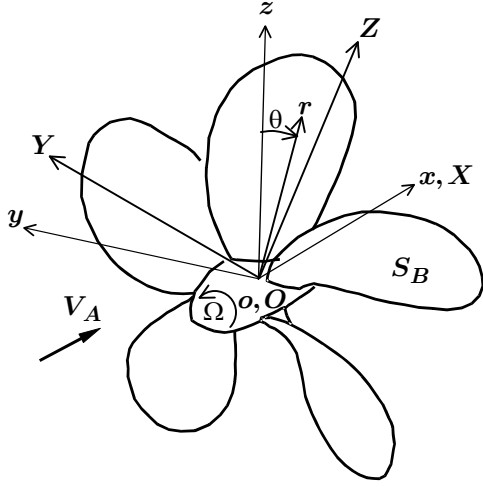


Figure 1 Coordinate systems of propeller

Next the mean camber surface is divided into M segments in the spanwise direction corresponding to the division of the source panels and divided into N_γ in the chordwise direction. Here we introduce ξ axis whose origin locates at the leading edge and is extended to the trailing vortex surface along the mean camber surface. The position of the bound vortex $\xi_{\mu\nu}^{LP}$ and control point $\xi_{\mu\nu}^{CP}$ on the mean camber surface are expressed by the following equations according to the QCM theory.

$$\begin{aligned} \xi_{\mu\nu}^{LP} &= \xi_L(r_\mu) + \frac{\xi_T(r_\mu) - \xi_L(r_\mu)}{2} \left(1 - \cos \frac{2\nu-1}{2N_\gamma} \pi \right) \\ \xi_{\mu\nu}^{CP} &= \xi_L(\bar{r}_\mu) + \frac{\xi_T(\bar{r}_\mu) - \xi_L(\bar{r}_\mu)}{2} \left(1 - \cos \frac{\nu}{N_\gamma} \pi \right) \end{aligned} \quad (3)$$

Where $\bar{r}_\mu = \frac{1}{2}(r_\mu + r_{\mu+1})$

μ and ν are numbers in the spanwise and chordwise directions. $\xi_L(r_\mu)$ and $\xi_T(r_\mu)$ are the positions of the leading edge(L.E.) and trailing edge(T.E.), respectively. And total $(M \times N_\gamma) \times K$ horse shoe vortices are located on the mean camber surface according to Equation (3) as illustrated in **Figure 2**. One set of ring vortices consists of one bound vortex, two free vortices and the first spanwise shed vortex CH closest to the trailing edge in the trailing wake. In the case of the unsteady problem the shed vortex flows out from T.E.. Thus the ring vortex, which represents the shed vortex, is located in the trailing wake. This ring vortex consists of two spanwise shed vortex CH, EF and two streamwise trailing vortex CE, HF. Here we define the induced velocity vector due to the ν -th ring vortex of unit strength which starts from the μ -th strip and ones due to the ℓ -th ring vortex of unit strength located in the trailing wake as $\bar{v}_{k\mu\nu}^\gamma$ and $\bar{v}_{k\mu\ell}^w$ respectively. These induced velocity vector are expressed as

$$\begin{aligned} \bar{v}_{k\mu\nu}^\gamma &= \bar{v}_{k\mu\nu}^B + \sum_{\nu'=v}^{N_\gamma} (\bar{v}_{k\mu+1\nu'}^F - \bar{v}_{k\mu\nu'}^F) - \bar{v}_{k\mu\ell}^{ws} \Big|_{\ell=1} \\ \bar{v}_{k\mu\ell}^w &= \bar{v}_{k\mu\ell}^{ws} - \bar{v}_{k\mu\ell+1}^{ws} + \bar{v}_{k\mu+1\ell}^{wc} - \bar{v}_{k\mu\ell}^{wc} \end{aligned} \quad (4)$$

Where

$\bar{v}_{k\mu\nu}^B$ = induced velocity vector due to the bound vortex of unit strength on the mean camber surface

$\bar{v}_{k\mu\nu}^F$ = induced velocity vector due to the free vortex of unit strength on the mean camber surface

$\bar{v}_{k\mu\ell}^{ws}$ = induced velocity vector due to the spanwise shed vortex of unit strength in the trailing wake

$\bar{v}_{k\mu\ell}^{wc}$ = induced velocity vector due to the streamwise trailing vortex of unit strength in the trailing wake

The induced velocity vector \bar{v} due to each line segment of vortex is calculated by the Biot-Savart law.

If we define the segments of the ring vortex on the mean camber surface at time t_L and the ring vortex in the trailing wake as $\gamma_{k\mu\nu}(t_L)$ and $\Gamma_{k\mu}(t_L)$, the induced velocity vector due to the vortex model of the QCM theory is given by the following equation.

$$\begin{aligned} \bar{V}_\gamma &= \sum_{k=1}^K \sum_{\mu=1}^M \sum_{\nu=1}^{N_\gamma} \gamma_{k\mu\nu}(t_L) \bar{v}_{k\mu\nu}^\gamma \Delta \xi_{\mu\nu} \\ &+ \sum_{k=1}^K \sum_{\mu=1}^M \sum_{\ell=1}^{L-1} \Gamma_{k\mu}(t_{L-\ell}) \bar{v}_{k\mu\ell}^w \end{aligned} \quad (5)$$

Where

$$\Delta \xi_{\mu\nu} = \frac{\pi c(\bar{r}_\mu)}{2N_\gamma} \sin \frac{2\nu-1}{2N_\gamma} \pi, \quad \Gamma_{k\mu}(t_L) = \sum_{\nu=1}^{N_\gamma} \gamma_{k\mu\nu}(t_L) \Delta \xi_{\mu\nu}$$

$c(\bar{r}_\mu)$: chord length of μ section

Equation (5) is used when the control points are on the mean camber surface. When the control points are on the blade surface, the ring vortices are close to the control points especially for thin wing. In this case we treat the ring vortices on the mean camber surface and shed vortex nearest to T.E. as the vortex surfaces in order to avoid numerical error. We call this treatment ‘‘Thin Wing Treatment’’ (Maita et al. 1996). Then we modify the vortex model of the QCM theory (**Figure 2(a)**) as follows:

First, we close the ring vortex on the mean camber surface at T.E. and locate ring vortices ABCH, HCDG and GDEF downstream from T.E. as illustrated in **Figure 2(b)**.

Next, we replace the ν -th ring vortex with a set of ring vortices distribution along $\Delta \xi_{\mu\nu}$ ($\xi_{\mu\nu-1}^{CP} \sim \xi_{\mu\nu}^{CP}$) on the mean camber surface as illustrated in the middle of **Figure 2(b)**. Then the ring vortex ABCH just downstream from T.E. and ring vortex HCDG are replaced with a set of ring vortices distribution along $\Delta \xi_\mu^w$ in the trailing wake. The other ring vortices from $\Delta \xi_\mu^w$ are calculated as discrete ring vortices.

In this case, the induced velocity vectors due to the vortex systems on the mean camber surface and trailing wake are expressed as

$$\begin{aligned}
\vec{V}_\gamma &= \sum_{k=1}^K \sum_{\mu=1}^M \sum_{v=1}^{N_\gamma} \gamma_{k\mu v}(t_L) \int_{\xi_{k\mu v-1}^{CP}}^{\xi_{k\mu v}^{CP}} \vec{v}_{k\mu}^\gamma(\xi) d\xi \\
&+ \sum_{k=1}^K \sum_{\mu=1}^M \sum_{v=1}^{N_\gamma} \gamma_{k\mu v}(t_L) \frac{\Delta \xi_{\mu v}^w}{\Delta \xi_{\mu}^w} \int_{\xi_{T(\bar{r}_\mu)}^w}^{\xi_{T(\bar{r}_\mu)} + \Delta \xi_{\mu}^w} \vec{v}_{k\mu}^{ABCH}(\xi) d\xi \\
&+ \sum_{k=1}^K \sum_{\mu=1}^M \Gamma_{k\mu}(t_{L-1}) \frac{1}{\Delta \xi_{\mu}^w} \int_{\xi_{T(\bar{r}_\mu)}^w}^{\xi_{T(\bar{r}_\mu)} + \Delta \xi_{\mu}^w} \vec{v}_{k\mu}^{HCDG}(\xi) d\xi \quad (6) \\
&+ \sum_{k=1}^K \sum_{\mu=1}^M \Gamma_{k\mu}(t_{L-1}) \vec{v}_{k\mu}^{GDEF} \\
&+ \sum_{k=1}^K \sum_{\mu=1}^M \sum_{\ell=2}^{L-1} \Gamma_{k\mu}(t_{L-\ell}) \vec{v}_{k\mu}^{\ell}
\end{aligned}$$

Where

$$\begin{aligned}
\vec{v}_{k\mu}^\gamma(\xi) &= \vec{v}_{k\mu}^B(\xi) + (\vec{v}_{k\mu+1}^F(\xi) - \vec{v}_{k\mu}^F(\xi)) \\
&+ \sum_{v'=v+1}^{N_\gamma} (\vec{v}_{k\mu+1v'}^F - \vec{v}_{k\mu v'}^F) - \vec{v}_{k\mu}^{AB} \\
\vec{v}_{k\mu}^{ABCH}(\xi) &= \vec{v}_{k\mu}^{AB} + \vec{v}_{k\mu+1}^{BC}(\xi) - \vec{v}_{k\mu}^{AH}(\xi) - \vec{v}_{k\mu}^{HC}(\xi) \\
\vec{v}_{k\mu}^{HCDG}(\xi) &= \vec{v}_{k\mu}^{HC}(\xi) + \vec{v}_{k\mu+1}^{CD}(\xi) - \vec{v}_{k\mu}^{HG}(\xi) - \vec{v}_{k\mu}^{GD} \\
\vec{v}_{k\mu}^{GDEF} &= \vec{v}_{k\mu}^{GD} + \vec{v}_{k\mu+1}^{DE} - \vec{v}_{k\mu}^{GF} - \vec{v}_{k\mu}^{FE}
\end{aligned}$$

Here the first term in the right hand side of Equation (6) is divided according to ‘‘Thin Wing Treatment’’, the second and third terms express the shed vortex just downstream from T.E. and the 4-th and 5-th terms express other ring vortices in the trailing wake.

In this way, the velocity vector \vec{V} around a propeller in the propeller coordinate system is expressed as

$$\vec{V} = \vec{V}_I + \vec{V}_\gamma + \vec{V}_m \quad (7)$$

Where \vec{V}_I , \vec{V}_γ and \vec{V}_m are inflow, induced velocity vectors due to vortex and source distributions, respectively.

The boundary conditions at the control points on the blade surfaces and mean camber surfaces are that there is no flow across the surfaces. Therefore the equation of the boundary condition is given as follow:

$$\begin{aligned}
\vec{V} \cdot \vec{n} &= 0 \\
&\text{on Wing and Camber Surface (except T.E.)} \quad (8) \\
\vec{V} \cdot \vec{n} &= V_N \quad \text{at T.E.}
\end{aligned}$$

Where \vec{n} is the normal vector on the blade surface and mean camber surfaces. V_N is the normal velocity at T.E. to satisfy the Kutta condition and expressed by the following equation.

$$V_N^{(i+1)} = \Delta p^{(i)} \beta / \left(\rho |\vec{V}_I| \right) + V_N^{(i)} \quad (9)$$

And i is the number of iteration. The first term in the right hand side in Equation (9) means the corrector for the value of the previous step $V_N^{(i)}$. V_N is proportional to the pressure difference Δp expressed as

$$\Delta p = \rho \frac{\partial}{\partial t} (\phi_+ - \phi_-) + \frac{1}{2} \rho (V_+^2 - V_-^2) \quad (10)$$

Here ϕ_+ and ϕ_- or V_+ and V_- mean the perturbation potential or the magnitude of velocity at the control points on the upper and the lower surface, which are closest to T.E.. The iteration is continued until Δp is small enough. β means the acceleration factor and $\beta = 1$ in this paper. ρ is the density of the fluid. The Kutta condition of unsteady SQCM is given by

$$\Delta p = 0 \quad (11)$$

On the other hand, we consider that the first equation in Equation (8) includes the Kutta condition.

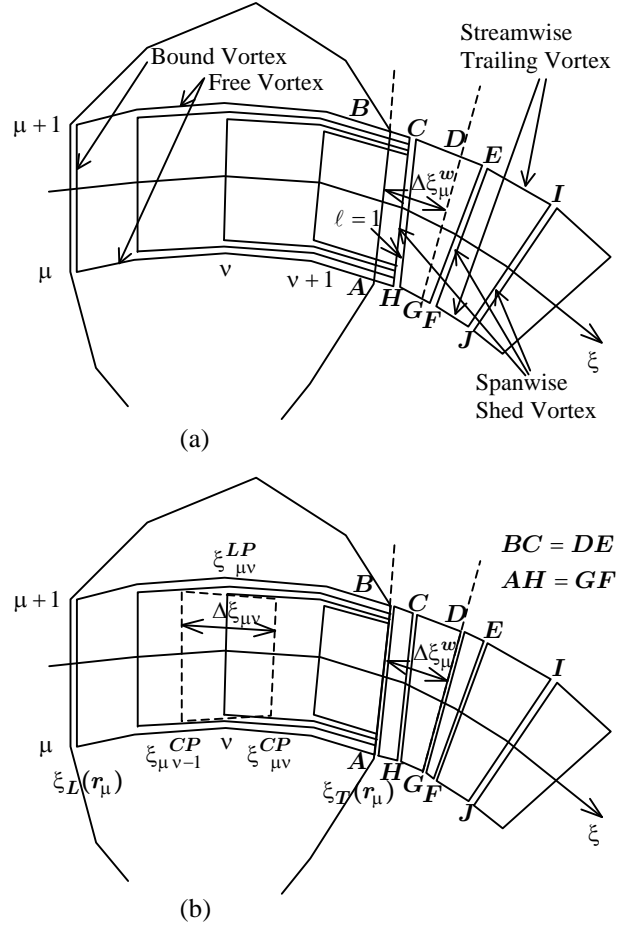


Figure 2 Arrangement of vortex system

The pressure $p(t)$ on the propeller blade is calculated by the unsteady Bernoulli equation expressed as

$$p(t) - p_0 = -\frac{1}{2} \rho \left(|\vec{V}|^2 - |\vec{V}_I|^2 \right) - \rho \frac{\partial \phi}{\partial t} \quad (12)$$

Where

p_0 = the static pressure in the undisturbed inflow

ϕ = the perturbation potential in the propeller coordinate system

Here the time derivative term of ϕ in Equation (12) is obtained numerically by two points upstream difference scheme with respect to time.

The pressure of the propeller blade is expressed as the following pressure coefficient C_{pn} in order to compare the calculated results with experimental data.

$$C_{pn} = \frac{p(t) - p_0}{\frac{1}{2} \rho n^2 D^2} \quad (13)$$

Where D is the diameter of the propeller.

The thrust T and the torque Q of the propeller are calculated by pressure integration. Denoting the X -, Y - and Z -components of the normal vector on the blade surface by n_X , n_Y and n_Z , respectively, the thrust and the torque are expressed by

$$\begin{aligned} T &= \iint_{S_B} (p(t) - p_0) n_X dS \\ Q &= \iint_{S_B} (p(t) - p_0) (n_Y Z - n_Z Y) dS \end{aligned} \quad (14)$$

Finally the advanced coefficient J , the thrust and the torque coefficients K_T , K_Q are expressed as follow:

$$J = \frac{V_A}{nD}, \quad K_T = \frac{T}{\rho n^2 D^4}, \quad K_Q = \frac{Q}{\rho n^2 D^5} \quad (15)$$

3 CALCULATION METHOD FOR CAVITATION

In the present method we assume that the pressure on the cavity surface is constant according to the free streamline theory. The difficulty in the analysis of the cavitating flow is that not only zero normal velocity condition but also constant pressure condition must be satisfied on the cavity surface. On the other hand the blade surface, which is not covered with cavity, must satisfy the zero normal velocity condition only. Therefore we must solve the mixed boundary value problem.

We adopt the cavitation number σ_v or σ_n corresponding to those of published experimental data to be referred in this paper. σ_v and σ_n are defined by

$$\sigma_v = \frac{p_0 - p_v}{\frac{1}{2} \rho V_A^2} \quad (16)$$

$$\sigma_n = \frac{p_0 - p_v}{\frac{1}{2} \rho n^2 D^2} \quad (17)$$

Where p_v = saturated vapor pressure

And we obtain the following relations.

$$V_T = \sqrt{|\vec{V}_I|^2 + \sigma_v V_A^2 - 2 \frac{\partial \phi}{\partial t}} \quad (18)$$

$$V_T = \sqrt{|\vec{V}_I|^2 + \sigma_n n^2 D^2 - 2 \frac{\partial \phi}{\partial t}} \quad (19)$$

The third term in the square root in Equation (18) and (19) is unknown. So this term makes the nonlinear cavity flow theory complicate. Needless to say that this term is excluded in the case of steady problem.

Here we describe the calculation procedure for cavitation.

(Step 1)

First of all we assume the initial cavity length ℓ_μ for each spanwise section. Next we give the cavitation number σ_v or σ_n to obtain the tangential velocity V_T , and then determine the source and vortex distributions from the following equation.

$$\frac{\Phi_{\mu v} - \Phi_{\mu v-1}}{\Delta s_{\mu v}} = V'_T \quad (20)$$

Here $\Phi_{\mu v}$ and $\Phi_{\mu v-1}$ are the total velocity potential on the control point of the v -th and $v-1$ -th cavity surface panels, respectively. $\Delta s_{\mu v}$ means the distance between these two control points (See **Figures 3** and **4**). In the case of unsteady problem, the initial cavity length and the initial value of potential can be assumed using the converged cavity shape at the previous time step. V'_T means the modified tangential velocity by considering the cross flow component V_{Cr} in the cylindrical coordinate system ($\vec{V}_C(V_{Cx}, V_{Cr}, V_{C\theta})$, \vec{V}_C : the velocity vector on the cavity surface) and is expressed by

$$V'_T = \sqrt{V_T^2 - V_{Cr}^2} \quad (21)$$

If we use V_T in the boundary condition on the cavity surface (Equation (20)), the pressure condition is satisfied two-dimensionally for chordwise section. But using V'_T , we get the following equation.

$$V_T = \sqrt{V_{Cx}^2 + V_{Cr}^2 + V_{C\theta}^2} \quad (22)$$

$$\text{Where } \sqrt{V_{Cx}^2 + V_{Cr}^2} = \frac{\Phi_{\mu v} - \Phi_{\mu v-1}}{\Delta s_{\mu v}}$$

Equation (22) means that the tangential velocity condition (the constant pressure condition) is satisfied three-dimensionally on the cavity surface.

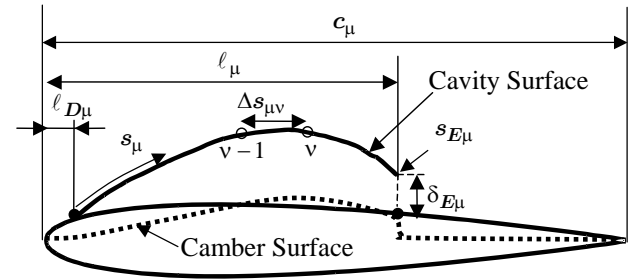


Figure 3 Model of a partially cavitating section

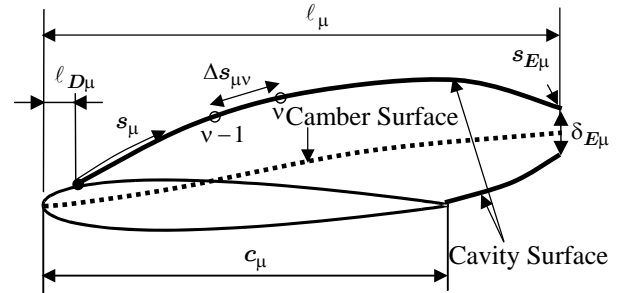


Figure 4 Model of a supercavitating section

We divide the cavity surface into even spacing panels in the chordwise direction. On the other hand, we divide the non-cavity surface on the blade into cosine spacing panels. The cavity detachment point $\ell_{D\mu}$ must be determined by the laminar separation point or the transition point for turbulence flow. But this is so difficult that we will treat the viscous effects in the future work.

Equation (8) is given on the blade surface, which is not covered with the cavity, and the mean camber surface. Here we consider the mean position between the back and face panels with the cavity surface to be the mean camber surface. Thus we can derive $(M \times (2N + N_\gamma)) \times K$ linear simultaneous equations which determine m and γ .

(Step 2)

When we calculate the velocity on the cavity surface using (Step 1), we can't generally satisfy the zero normal velocity condition on the cavity surface. Therefore we need to arrange the source panels so as to coincide with the flow direction using the following equation.

$$V_T \frac{\partial h}{\partial s} + \frac{\partial h}{\partial t} = \vec{V} \cdot \vec{n} \quad (23)$$

Here s (s_μ) represents the distance from the cavity detachment point along the cavity surface (See **Figures 3** and **4**) and h means the cavity thickness. Discretizing Equation (23), the cavity height of the v -th panel $h_{\mu v}(t)$ is expressed by

$$h_{\mu v}(t) = \frac{\vec{V} \cdot \vec{n} + \frac{V_T}{\Delta s_{\mu v}} h_{\mu v-1}(t) + \frac{h_{\mu v}(t - \Delta t)}{\Delta t}}{\frac{V_T}{\Delta s_{\mu v}} + \frac{1}{\Delta t}} \quad (24)$$

Where Δt means time step.

In the case of steady problem, $h_{\mu v}$ is expressed by

$$h_{\mu v} = h_{\mu v-1} + \frac{\vec{V} \cdot \vec{n}}{V_T} \Delta s_{\mu v} \quad (25)$$

Then the opening of the cavity end $\delta_{E\mu}$ is obtained by the integration of Equation (24) or (25) along s .

(Step 3)

We repeat (Step 1) and (Step 2) until the cavity shape converges.

(Step 4)

After the cavity shape converges, we compare $\delta_{E\mu}$ with the target value $\delta_{ET\mu}$ and adjust the cavity length ℓ_μ by using the following equation.

$$\ell_\mu^{(n+1)} = \ell_\mu^{(n)} + w(\delta_{ET\mu} - \delta_{E\mu}) \quad (26)$$

Here n and w are the iteration number for adjusting the cavity length and a proper weight coefficient, respectively. We adopt the small value for $\delta_{ET\mu}$ as long as the cavity shape converges smoothly. As the result, the solutions by our method are similar to those of closed model. When ℓ_μ is close to the chord length at the section, it is difficult to calculate the cavity shape smoothly. Therefore we shift the section from the

partially cavitating model (**Figure 3**) to the supercavitating model (**Figure 4**) when ℓ_μ exceeds $1.02c_\mu$ in Equation (26).

(Step 5)

We repeat described procedures until the cavity length satisfies the following condition at all spanwise sections.

$$\left| \ell_\mu^{(n+1)} - \ell_\mu^{(n)} \right| \leq 0.01c_\mu \quad (27)$$

(Step 6)

After the cavity length converges at all spanwise section, we calculate the thrust and the torque by Equation (14). Here we integrate the pressure on the blade surface even on the cavity area by using $-\sigma_n$.

4 CALCULATED RESULTS

4.1 Steady Problem

We select M.P.No.123 propeller and M.P.No.125 propeller for the calculations. Both of these propellers were developed by Ship Research Institute in Japan (SRI, present National Maritime Research Institute) and cavitation tests were conducted at SRI (Kadoi et al. 1978). The principal particulars of these propellers are shown in **Table 1**. Only the pitch ratios are different between M.P.No.123 and M.P.No.125.

Table 1 Principal particulars of propellers

NAME OF PROPELLER	M.P.No.123	M.P.No.125
DIAMETER(m)	0.250	0.250
NUMBER OF BLADE	6	6
PITCH RATIO AT 0.7R	1.264	1.750
EXPANDED AREA RATIO	0.8	0.8
HUB RATIO	0.18	0.18
RAKE ANGLE(DEG.)	7.3	7.3
BLADE SECTION	SRI-a	SRI-a

Panel arrangements of propeller are shown in **Figure 5**. The propeller blade surface including cavity surface are divided into 30 panels in the chordwise direction (3 panels from leading edge to $\ell_{D\mu}$, 15 panels from $\ell_{D\mu}$ to ℓ_μ and 12 panels from ℓ_μ to c_μ in the case of partial cavitation, 3 panels from leading edge to $\ell_{D\mu}$, 15 panels from $\ell_{D\mu}$ to c_μ and 12 panels from c_μ to ℓ_μ in the case of super cavitation) and divided into 20 panels in the spanwise direction. Camber surface is divided into 31 segments in the chordwise direction. **Figure 5** shows the panel arrangements in the case of non-cavitation at all sections. Here we ignore the hub surface.

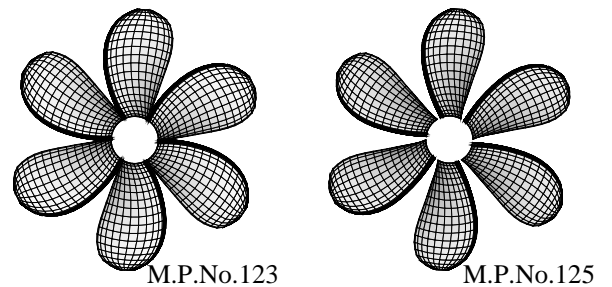


Figure 5 Panel arrangements for SRI-a propellers

Figures 6 and 7 show the cavitation patterns of M.P.No.123 and M.P.No.125 comparing with the experimental data. The calculated results agree well with the experimental data.

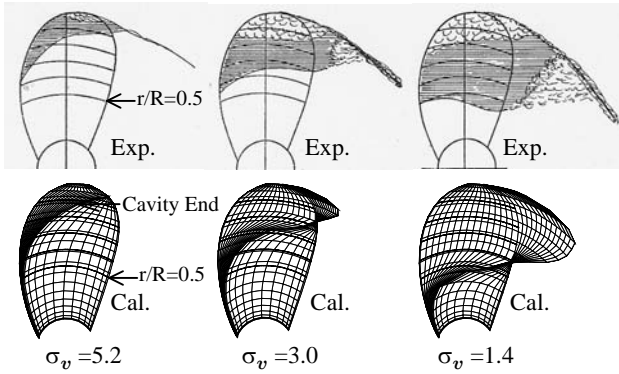


Figure 6 Cavitation patterns (M.P.No.123, $J=0.7$)

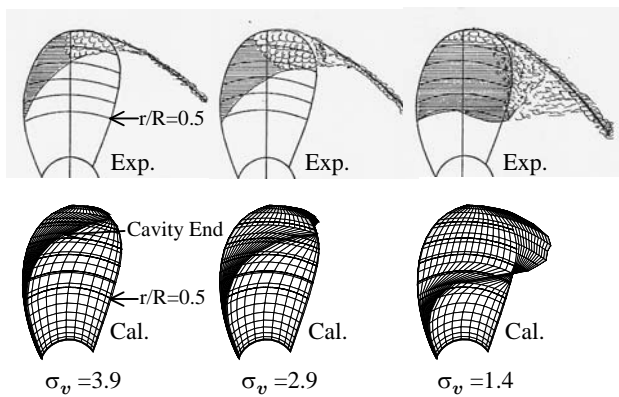


Figure 7 Cavitation patterns (M.P.No.125, $J=1.0$)

Figure 8 shows the comparisons of the pressure distributions on the blade and cavity surfaces to investigate the effects of the cross flow consideration. The results with cross flow show the good agreement with negative cavitation number which is the target pressure coefficient on the cavity surface. On the other hand, the calculated results without cross flow don't satisfy the constant pressure condition sufficiently.

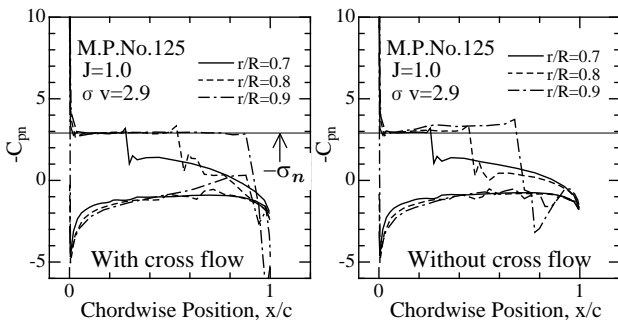


Figure 8 Cavity thickness with and without cross flow

Figures 9 and 10 show the thrust coefficient K_T and the torque coefficient K_Q of M.P.No.123 and M.P.No.125 comparing with the experimental data (Kadoi et al. 1978). In these figures, experimental data and calculated results without cavitation are also shown. The viscous effects are

not considered in all calculated results. The calculated thrust and torque coefficients decrease abruptly at a low advance coefficient as shown in experimental data. We emphasize that the calculated peak points of K_T and K_Q agree with experimental data in most cases. In the case of low cavitation number, the agreements of the peak points are not so well. One of the reasons is that the boundary between cavity area and non-cavity area can't be expressed by the present panel division method. Also, we have to determine the cavity detachment point theoretically in order to simulate the cavity accurately near the root.

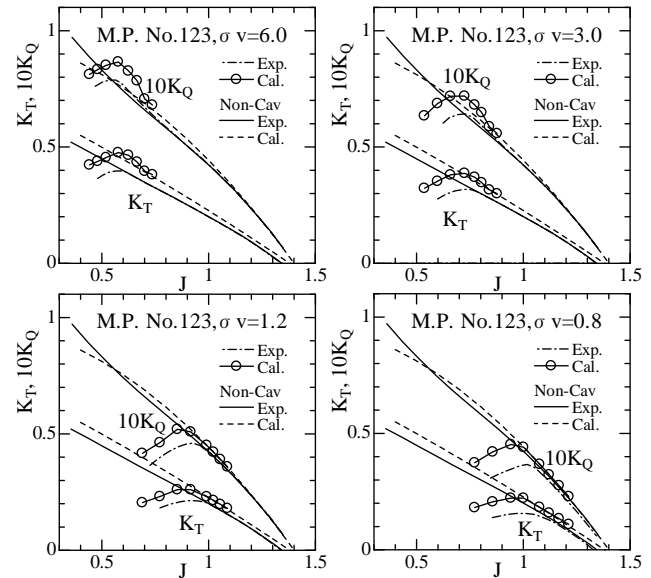


Figure 9 Thrust and torque coefficients (M.P.No.123)

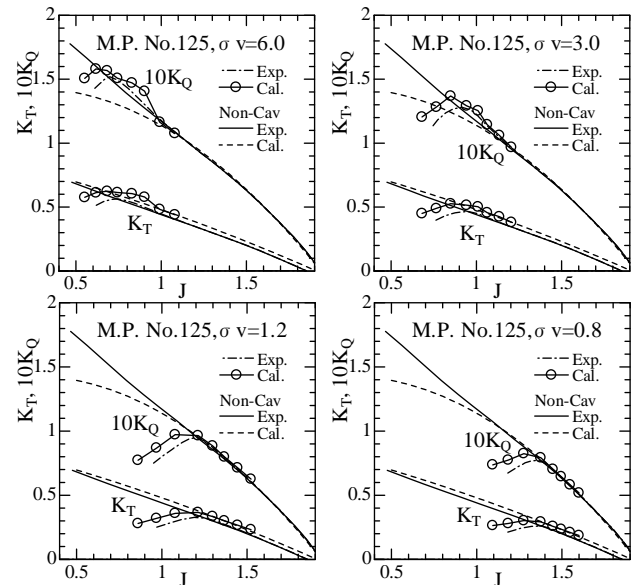


Figure 10 Thrust and torque coefficients (M.P.No.125)

4.2 Unsteady problem

We select conventional propeller (CP) and highly skewed propeller (HSP) of Seiyun-Marui in order to compare the experimental data at SRI (Kudo et al. 1989). The experimental data were obtained by a highly advanced

method of measuring the three dimensional cavity shape using a laser beam coupled with a CCD (Charge Coupled Device) camera and image processor. **Table 2** shows the principal particulars and **Figure 11** shows the panel arrangements of these propellers. The time step Δt is given by the following equation.

$$\Delta t = \Delta\theta / 360.0 / n \quad (28)$$

Where $\Delta\theta$ is chosen as $\Delta\theta=2.5$ degrees. Calculations are performed using the wake distribution (see **Figure 12**) given by the reference (Kudo et al. 1989). Panel division method and other treatments are the same in the steady case described in 4.1.

Table 2 Principal particulars of propellers (Seiun-Maru-I)

NAME OF PROPELLER	CP	HSP
DIAMETER (m)	0.22095	0.2200
NUMBER OF BLADE	5	5
PITCH TARIO AT 0.7R	0.95	0.944
EXPANDED AREA RATIO	0.650	0.700
HUB RATIO	0.1972	
RAKE ANGLE (DEG.)	6.0	-3.03
BLADE SECTION	MAU	Modified SRI-B

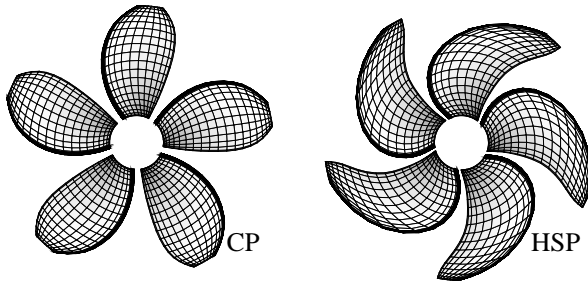


Figure 11 Panel arrangements for Seiun-Maru-I propellers

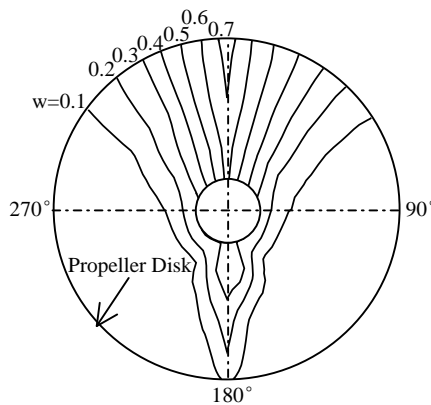


Figure 12 Axial wake velocity distribution

Figures 13 and 14 show the calculated cavitation patterns of CP and HSP. The cavity end lines by experimental sketch are added in these figures. We can see the good agreements between calculated results and experimental data in both CP and HSP.

Figures 15 and 16 show the calculated cavity shape of CP and HSP comparing with experimental data. In the figures of $r/R=0.95$, we added the calculated results without cross flow component. In the calculation without cross flow component, following equation is used instead of Equation (20).

$$\frac{\Phi_{\mu\nu} - \Phi_{\mu\nu-1}}{\Delta s_{\mu\nu}} = V_T \quad (29)$$

The differences of calculated results with and without cross flow are small with regard to CP. In HSP, the calculated cavity shapes considering cross flow effect agree well with the experimental data.

Figures 17 and 18 show the variations of cavity area and cavity volume with regard to both of CP and HSP comparing with experimental data. In these figures, we also show the calculated results without cross flow. Calculated results with cross flow can express the characteristic of variations and the differences between CP and HSP qualitatively.

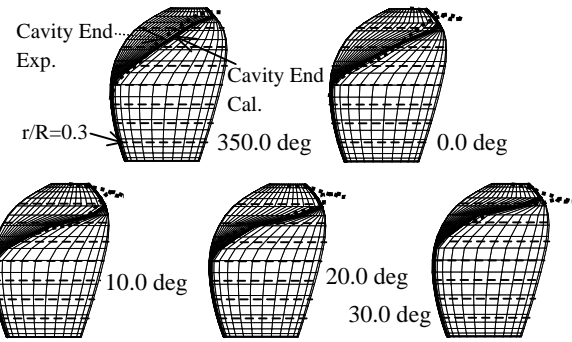


Figure 13 Cavitation patterns (CP, $K_T=0.207$, $\sigma_n=3.06$)

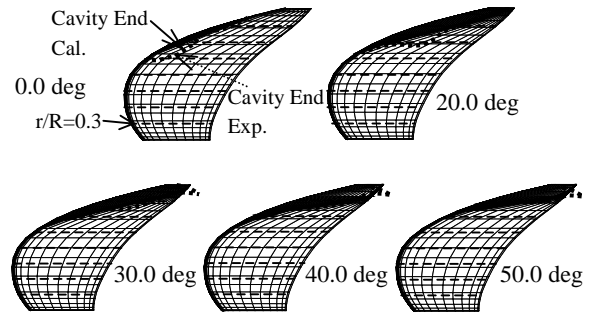


Figure 14 Cavitation patterns (HSP, $K_T=0.201$, $\sigma_n=2.99$)

5 CONCLUSIONS

In this paper we presented a calculation method for steady and unsteady cavitating propeller using a simple surface panel method "SQCM". We considered the cross flow velocity in the boundary condition on the cavity surface. Comparison between the calculated results and experimental data led the following conclusions:

- (1) The present method can predict the thrust and the torque in extensive advance coefficients and cavitation numbers. In unsteady case, the present method can express the variations of the cavity area and cavity volume.
- (2) The cross flow effect on the cavity surface gives reasonable cavity shapes and variations of cavity area and volume especially in HSP.

- (3) The viscous effect on the cavity detachment point should be considered in order to improve the accuracy of calculation.

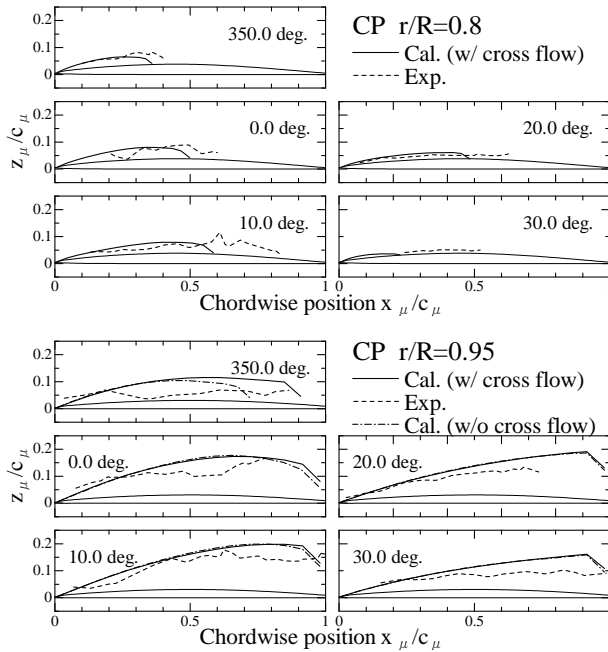


Figure 15 Cavity shapes (CP, $K_T=0.207$, $\sigma_n=3.06$)

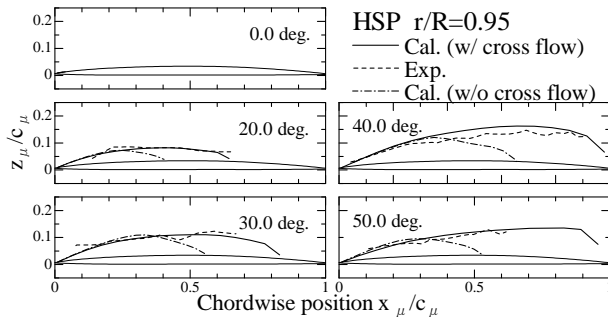


Figure 16 Cavity shapes (HSP, $K_T=0.201$, $\sigma_n=2.99$)

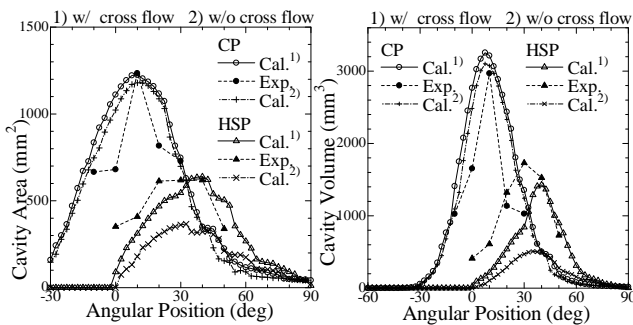


Figure 17 Variations of cavity area and volume
(CP : $K_T=0.207$, $\sigma_n=3.06$, HSP : $K_T=0.201$, $\sigma_n=2.99$)

REFERENCES

- Ando, J., Maita, S. and Nakatake, K. (1998). 'A New Surface Panel Method to Predict Steady and Unsteady Characteristics of Marine Propeller'. Proceedings of 22st Symposium on Naval Hydrodynamics, Washington D.C., pp.142-154.
- Ando, J., Matsumoto, D., Maita, S., Ohashi, K. and Nakatake, K. (1999). 'Calculation of Three-Dimensional Steady Cavitation by a Simple Surface Panel Method'. Journal of the Society of Naval Architects of Japan, Vol.186, pp.17-27.
- Ando, J., Kanemaru, T., Ohashi, K. and Nakatake, K. (2000). 'Calculation of Three-Dimensional Unsteady Sheet Cavitation by a Simple Surface Panel Method'. Journal of the Society of Naval Architects of Japan, Vol.188, pp.91-103.
- Fine, N.E. (1992). 'Nonlinear Analysis of Cavitating Propellers in Nonuniform Flow'. Ph.D. Thesis, M.I.T., Cambridge, Mass.
- Hess, J.L. and Smith, A.M.O. (1964). 'Calculation of Nonlifting Potential Flow about Arbitrary Three Dimensional Bodies'. Journal of Ship Research, Vol. 8, No. 2, pp.22-44.
- Kadoi, H., Kokubo, Y., Koyama, K. and Okamoto, M. (1978). 'Systematic Tests on the SRI-a-Propeller'. Report of the SRI, Vol.15, No.2.
- Kanemaru, T., Ando, J. (2008). 'Numerical Analysis of Steady Sheet Cavitation on a Marine Propeller Using a Simple Surface Panel Method "SQCM" '. Proceeding of 3rd PAAMES and AMEC2008, pp.25-34.
- Kim, Y.-G., Lee, C.-S. and Suh, J.-C. (1996). 'Prediction of Unsteady Performance of Marine Propellers with Cavitation Using Surface-Panel Method'. Proceedings of 21st Symposium on Naval Hydrodynamics, Trondheim, pp.913-929.
- Kinnas, S.A. and Fine, N.E. (1992). 'A Numerical Nonlinear Boundary Element Method for the Analysis of Unsteady Propeller Sheet Cavitation'. Proceedings of 19th Symposium on Naval Hydrodynamics, Seoul, pp.717-733.
- Kinnas, S.A. and Fine, N.E. (1993). 'A Numerical Nonlinear Analysis of the Flow around 2-D and 3-D Partially Cavitating Hydrofoils'. Journal of Fluid Mechanics, Vol. 254, pp.151-181.
- Kudo, T., Ukon, Y., Kurobe, U. and Tanibayashi, H. (1989). 'Measurement of Shape of Cavity on a Model Propeller Blade'. Journal of the Society of Naval Architects of Japan, Vol.166, pp.93-103.
- Lan, C.E. (1974). 'A Quasi-Vortex-Lattice Method in Thin Wing Theory'. Journal of Aircraft, Vol. 11, No. 9, pp.518-527